NJC

COMMUNICATION

Check for updates

A large-Stokes shift styryl pyridinium derivative with a stable green-light emission for imaging mitochondria in live cells†

Chathura S. Abeywickrama, [iD] *[a] Kavinda M. Arachchige,[a]
Kaveesha J. Wijesinghe, [iD] [b] Robert V. Stahelin [iD] [c] and Yi Pang [iD] [d]

A green-light-emitting styryl pyridinium probe (EPN) was developed for live-cell imaging applications. EPN exhibited a large Stokes shift ($\Delta\lambda \approx 150$ nm), due to an efficient ICT across the π–acceptor system. The probe exhibited exceptional biocompatibility and excellent specificity for cellular mitochondria. EPN exhibited great photostability to continuous irradiation and exhibited stable emission in cells up to 5 hours post-staining.

Small-molecule fluorescent imaging dyes are versatile tools for visualizing complex biological environments.[1–4] Recent advancements in fluorescence microscopy techniques that reach high spatial resolution (*i.e.*, super-resolution) have unlocked the potential of biomedical imaging at the molecular level.[5–7] Long-lasting, bright, and highly biocompatible imaging dyes are ideal for visualizing living systems. Probes with well-resolved excitation–emission profiles (*i.e.*, large Stokes shifts) can effectively mitigate issues such as self-quenching of the fluorophore and bleed-through interferences that occur during imaging.[4,8] Recently, several interesting large-Stokes shift ($\Delta\lambda \approx 100$–200 nm) imaging dyes for the red to near-infrared emission region have been developed.[9–12] Excited-state intra-molecular proton transfer (ESIPT) and intramolecular charge transfer (ICT) are two key photophysical phenomena that have been utilized to develop such large-Stokes shift imaging dyes.[4,13,14] Undoubtedly, the development of red-light- and NIR-emitting probes has distinct advantages in biomedical imaging research due to their relatively high ability to penetrate biological tissues. However, many imaging experiments demand multi-color fluorescent labels to distinguish multiple components in complex biological environments.
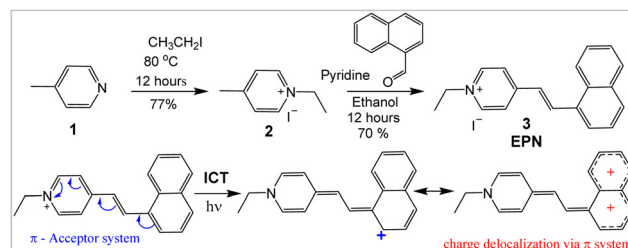
Therefore, the development imaging probes with favourable properties for imaging in the blue-green region is still critical for visualization purposes. Many available blue-green-light-emitting imaging dyes exhibit inherently narrow Stokes shifts ($\Delta\lambda < 20$ nm) and high cytotoxicity—as well as weak photo-stability, which limits their application in long-duration imaging sessions. Here, we report an interesting green-light-emitting π–acceptor (π–A)-type imaging probe (EPN) with a large Stokes shift ($\Delta\lambda \approx 100$–150 nm) for imaging mitochondria in live cells. EPN exhibited excellent photostability and biocompatibility and may be considered as a promising imaging candidate.

Synthesis

EPN (3) was synthesized in good yields by performing condensation of 1-napthaldehyde with pyridinium salt 2 as shown in Scheme 1. EPN was characterized using NMR spectroscopy and high-resolution mass spectrometry (Fig. S1, ESI†).

Optical properties

Photophysical properties of EPN in various solvents were studied and are summarized in Table 1 and Fig. 1. The absorbance spectra were acquired at $\lambda_{abs} \approx 370$–395 nm (Table 1). The absorbance signal of EPN exhibited a moderate blue shift in polar solvents (*i.e.*, $\lambda_{abs} \approx 370$ in water) in comparison to

[a] Department of Pharmaceutical Sciences, University of Connecticut, Storrs, CT 06269, USA. E-mail: chathura.abeywickrama@uconn.edu

[b] Department of Chemistry, University of Colombo, Colombo 00300, Sri Lanka

[c] Borch Department of Medicinal Chemistry and Molecular Pharmacology, Purdue University, West Lafayette, IN 47907, USA

[d] Department of Chemistry, University of Akron, OH 44325, USA

† Electronic supplementary information (ESI) available. See DOI: https://doi.org/10.1039/d4nj05398b

Scheme 1 Synthesis and intramolecular charge transfer (ICT) in EPN.

Table 1 Photophysical properties of **EPN**

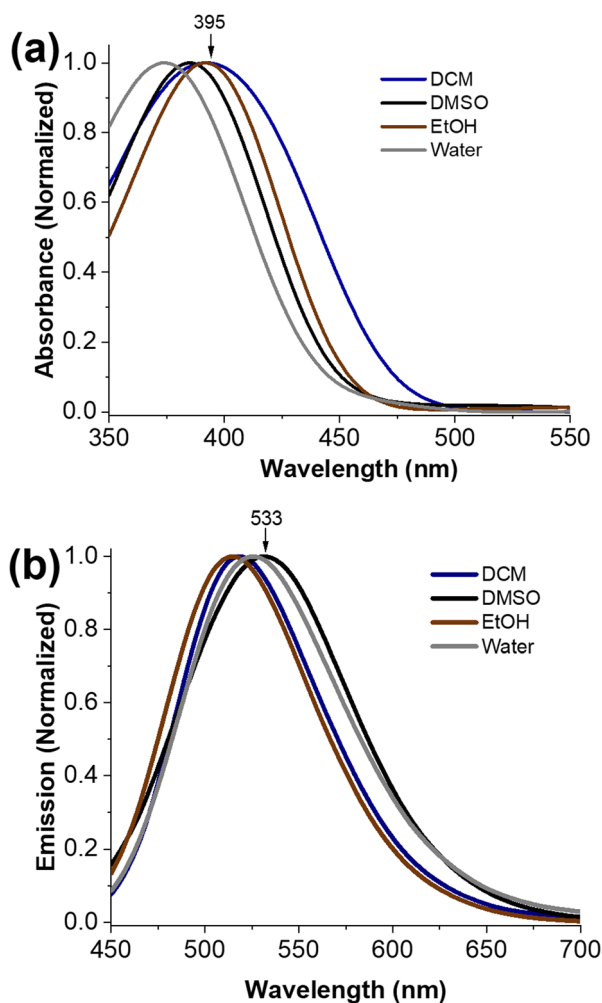| Solvent	Toluene	DCM	CHCl$_3$	DMSO	EtOH	Water
λ_{abs} (nm)	390	395	394	388	391	373
λ_{em} (nm)	490	518	507	533	514	525
$\Delta\lambda$ (nm)	100	123	113	145	123	152
ϕ_{fl}	0.002	0.025	0.018	0.036	0.044	0.011
ε(M^{-1} cm^{-1})	8172	10458	10940	9888	10170	9426

Fig. 1 (a) Absorbance and (b) emission spectra of **EPN** (1×10^{-5} M) in indicated solvent environments a 25 °C. **EPN** was excited with 390-nm-wavelength light and the emissions were collected from 420 nm to 700 nm.

non-polar solvents (*i.e.*, $\lambda_{abs} \approx 395$ in DCM), indicating a hypsochromic character (Fig. 1a). However, the emission of light from **EPN** did not exhibit such noticeable trend (Fig. 1b); this emission was found to be in the λ_{em} range 490–533 nm (*i.e.*, blue-green region) with calculated fluorescent quantum yields (φ_{fl}) of 0.002–0.044 (Table 1). In comparison to the emission of light from **EPN** in other solvents, that in toluene was found to be significantly weaker ($\varphi_{fl} \approx 0.002$), which can be explained by considering the characteristic "collisional quenching" properties of the solvent due to strong vibrational relaxations. The calculated Stokes shift ($\Delta\lambda$) values of **EPN** in environments

ranging from non-polar to polar were determined to respectively range from ≈ 100 to 150 nm, indicative of a stronger ICT effect in the polar solvent environments that increased the Stokes shift.

Low-temperature studies

The large Stokes shift of **EPN** ($\Delta\lambda \approx$ 100–150 nm) can be attributed to the extended conjugation across naphthalene, which further stabilized strong intramolecular charge transfer (ICT) from naphthalene (π-system) to the styryl pyridinium acceptor group as shown in Scheme 1. To evaluate the impact of the ICT, an ethanolic solution of **EPN** was frozen in liquid nitrogen to limit the molecular motion and bond rearrangements associated with the ICT process. While **EPN** was frozen under the ethanol matrix at an ultra-low temperature (*i.e.*, −188 °C), the probe exhibited an emission at $\lambda_{em} \approx 456$ nm (Fig. 2). When the temperature was increased to room temperature (*i.e.*, 25 °C), the emission peak was red-shifted to $\lambda_{em} \approx 514$ nm (Fig. 2). The observed large spectral
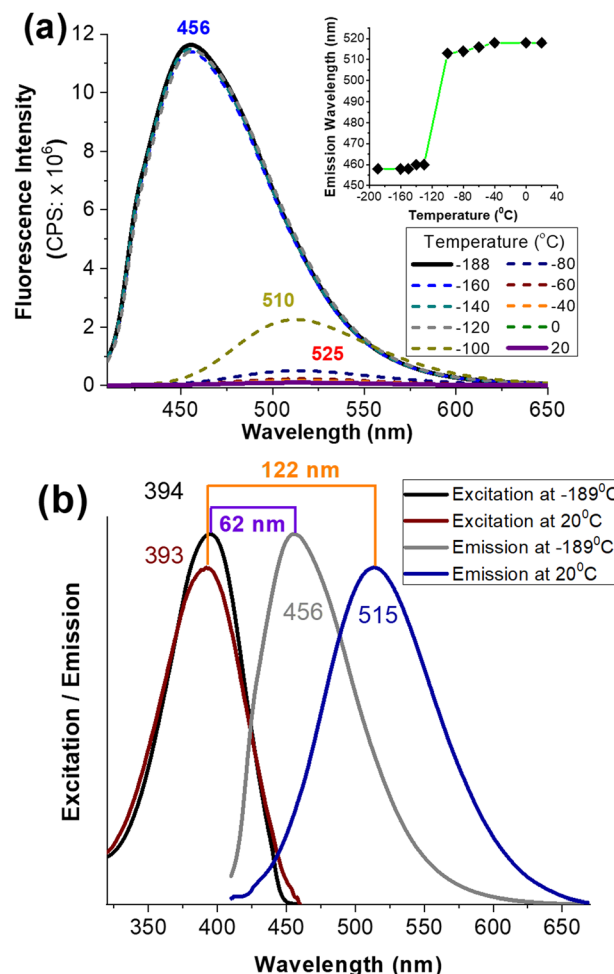

Fig. 2 (a) Fluorescence spectra of **EPN** (1×10^{-6} M) in EtOH at indicated temperatures. Inset at the top shows the emission of **EPN** as a function of temperature. **EPN** was excited at 390 nm to acquire the emission. (b) Normalized excitation and fluorescence spectra at indicated temperatures for **EPN** (1×10^{-6} M) in EtOH.

shift ($\Delta\lambda \approx 58$ nm, from 456 nm to 514 nm) in response to the temperature change indicated the impact of a strong ICT interaction (Scheme 1).

Live-cell imaging

The observed interesting photophysical properties encouraged us to investigate the potential of **EPN** to serve as a live-cell imaging probe. Thus, HepG2 cells (human hepatocellular carcinoma cell line) and A-172 cells (human glioblastoma cell line) were stained with **EPN** (2–4 μM) and visualized using fluorescence confocal microscopy (Fig. 3 and Fig. S6, S7, ESI†). Interestingly, cells stained with **EPN** exhibited a strong emission signal while exhibiting a non-uniform tubular network-like staining pattern, indicative of internalization into a specific cellular compartment. The resulting fluorescence confocal microscopy images did not exhibit a noticeable background signal, which suggested the suitability of the probe as a potential imaging dye. Based on our familiarity with the observed imaging pattern, we hypothesized that **EPN** became internalized into cellular mitochondria. The positively charged nature of **EPN** further supported our hypothesis, as many positively charged fluorescent dyes have exhibited the potential to localize into cellular mitochondria.

To confirm the subcellular specificity of **EPN**, fluorescence confocal microscopy colocalization imaging experiments were performed using HepG2 cells in the presence of a commercial mitochondrial marker (*i.e.*, MitoTracker™ Red FM: $\lambda_{ex} \approx 579$ nm, $\lambda_{em} \approx 579$ nm). **EPN** exhibited an excellent colocalization (calculated Pearson's colocalization constant = 0.9) with MitoTracker™ Red (Fig. 4), indicative of excellent specificity of the probe for mitochondria and hence providing compelling evidence to support its application as a versatile mitochondrial imaging probe. Considering the well-resolved excitation and emission spectral profiles ($\lambda_{ex} \approx 400$ nm, $\lambda_{em} \approx 520$ nm) that produced a large Stokes shift ($\Delta\lambda \approx 100$–150 nm) due to a strong ICT effect, **EPN** can be efficiently co-stained with any blue-green-light- to red-light-emissive fluorescent marker ($\lambda_{ex} \approx$ range from 450 nm to 700 nm) without producing any signal interference (*i.e.*, channel bleeding). **EPN** also exhibited exceptional stability in live-cell imaging where the probe was evaluated for imaging mitochondria in HepG2 cells for up to 5 hours (Fig. 5). The probe exhibited a stable emission
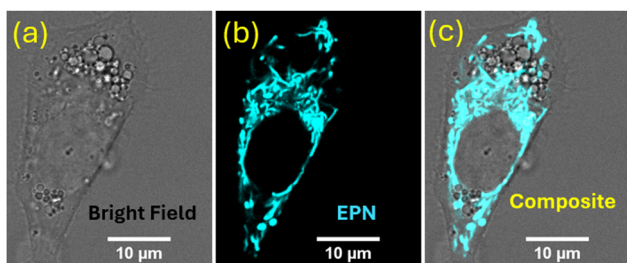

Fig. 4 Fluorescence confocal microscopy images of HepG2 cells stained with MitoTracker™ Red FM (200 nM) and **EPN** (4 μM), specifically (a) MitoTracker™ Red FM, (b) **EPN**, (c) bright field, (d) merging of two dyes, (e) composite image, (f) colocalization map, and (g)–(h) zoomed-in images of (d) and (e), respectively. MitoTracker™ Red FM was excited with 570-nm-wavelength light and the emissions were collected from 580 nm to 700 nm. **EPN** was excited with a 405-nm-wavelength laser line and emissions were collected from 480 nm to 560 nm.

from stained cells without any noticeable reduction in emission signal intensity (Fig. 5a). To further evaluate the photostability of the probe, HepG2 cells stained with **EPN** (4 μM) were continuously irradiated with a 405-nm-wavelength laser line (0.4 mW power) at 2-minute intervals for up to 30 minutes. Based on the collected fluorescence microscopy images, the percentage fluorescence recovered (average) was plotted as a function of the irradiation time (Fig. 5b). The calculated percentage recovery of the fluorescence was found to be over $\sim 85\%$ for **EPN** after 16 irradiation cycles, which provided convincing evidence of its high photostability as a blue-green imaging dye. To further validate the suitability of **EPN** for live-cell imaging experiments, the biocompatibility of the probe was evaluated by taking cell viability measurements (Fig. 5c). Interestingly, based on the viability assessment, **EPN** did not exhibit any noticeable cytotoxicity at concentrations of up to 10 μM, confirming the suitability of the probe as a biocompatible mitochondrial marker. Also, the laser

Fig. 3 Fluorescence confocal microscopy images of HepG2 cells stained with **EPN** (4 μM) for 30 minutes. Stained cells were excited with a 405-nm-wavelength laser line and the emissions with wavelengths from 480 nm to 560 nm were collected.
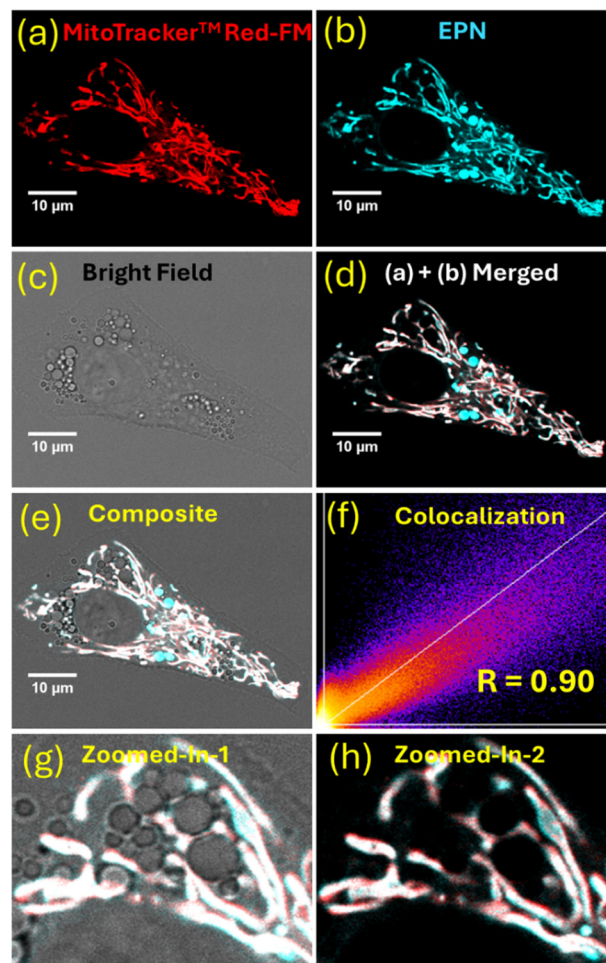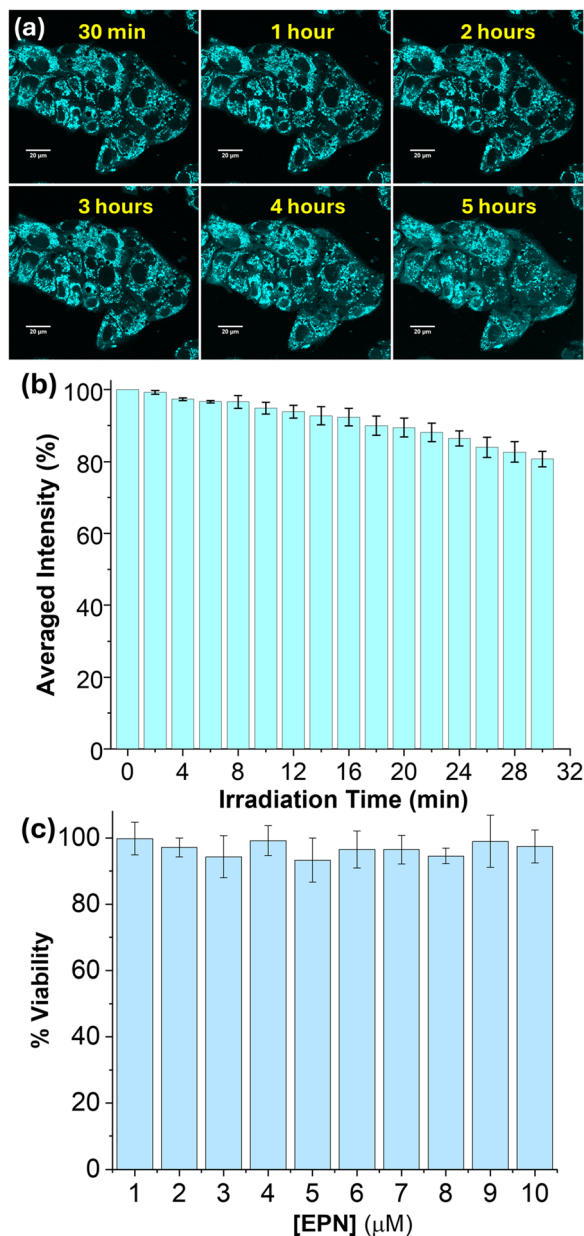
Fig. 5 (a) Fluorescenceconfocal microscopy images of HepG2 cells stained with **EPN** (4 μM). Images were obtained for experiments carried out for up to 5 hours. Scale bar denotes 10 μm. (b) Averaged fluorescence intensity (recovered) calculated after the continuous irradiation of **EPN** (4 μM)-stained cells for 30 minutes. (c) Cell viability data obtained for **EPN** using the CellTiter-Glo® Luminescent Cell Viability Assay.

irradiation (405 nm) experiments performed using **EPN**-stained A-172 cells did not show any noticeable morphological changes in bright-field or dark-field confocal microscopy images, suggesting no potential phototoxicity effect at current staining concentrations (Fig. S8, ESI†).

Conclusions

In summary, a highly biocompatible blue-green-light-emitting pyridinium-based styryl dye (**EPN**) was synthesized in good

yields for visualizing mitochondria in live cells. **EPN** exhibited a large Stokes shift ($\Delta\lambda > 100$ nm) due to strong ICT occurring *via* the π–acceptor system. The impact of the ICT was studied extensively by carrying out low-temperature fluorescence experiments, the results of which confirmed the contribution of ICT to the observed large Stokes shift. **EPN** was readily excitable with a commercially available laser line (*i.e.*, 405 nm), which produced a blue-green visualization of stained HepG2 cells. The excellent specificity of **EPN** for mitochondria was confirmed by the results of fluorescence-microscopy-based colocalization studies (calculated Pearson's colocalization constant = 0.9). **EPN** also exhibited the ability to produce a stable fluorescence signal from stained cells for long time periods (*i.e.*, up to 5 hours), confirming its suitability as a long-duration imaging probe. **EPN** was exposed to continuous laser irradiation (405 nm) to assess its photostability, and the probe exhibited over ~85% fluorescence recovery after 30 minutes, indicative of excellent photostability. A cell viability assessment also provided supporting evidence to confirm the biocompatibility of **EPN** for live-cell imaging experiments. Due to its structural simplicity, well-resolved excitation/emission profiles, excellent photostability and biocompatibility, **EPN** may be considered a promising small-molecule imaging probe for biomedical imaging applications.

Author contributions

Conceptualization, C. S. A.; methodology, C. S. A., Y. P., R. V. S., K. J. W., and K. M. A.; validation, C. S. A., K. J. W., and K. M. A.; formal analysis, C. S. A.,K. M. A., and K. J. W.; investigation, C. S. A.,K. M. A., and K. J. W.; resources, C. S. A., Y. P., and R. V. S.; data curation, C. S. A., K. J. W., and K. M. A.; writing – original draft preparation, C. S. A, and K. J. W.; writing – review and editing, C. S. A., and K. J. W.; supervision, C. S. A., Y. P., R. V. S., and K. J. W.; project administration, C. S. A.; funding acquisition, C. S. A. All authors have read and agreed to the published version of the manuscript.

Data availability

The data supporting this article have been included as part of the ESI.†

Conflicts of interest

There are no conflicts to declare.

Acknowledgements

Notes and references

1 G. Y. Wiederschain, *Biochemistry*, 2011, **76**, 1276–1277.

2 J. Zhang, R. E. Campbell, A. Y. Ting and R. Y. Tsien, *Nat. Rev. Mol. Cell Biol.*, 2002, **3**, 906.

3 M. S. T. Gonçalves, *Chem. Rev.*, 2008, **109**, 190–212.

4 C. S. Abeywickrama, *Chem. Commun.*, 2022, **58**, 9855–9869.

5 G. Jacquemet, A. F. Carisey, H. Hamidi, R. Henriques and C. Leterrier, *J. Cell Sci.*, 2020, **133**, jcs240713.

6 M. Fernández-Suárez and A. Y. Ting, *Nat. Rev. Mol. Cell Biol.*, 2008, **9**, 929.

7 M. V. Sednev, V. N. Belov and S. W. Hell, *Methods Appl. Fluoresc.*, 2015, **3**, 42004.

8 Z. Zhang, G. Zhang, J. Wang, S. Sun and Z. Zhang, *Comput. Theor. Chem.*, 2016, **1095**, 44–53.

9 N. I. Wickramasinghe, B. Corbin, D. Y. Kanakarathna, Y. Pang, C. S. Abeywickrama and K. J. Wijesinghe, *Biosensors*, 2023, **13**, 799.

10 L. Yuan, W. Lin and H. Chen, *Biomaterials*, 2013, **34**, 9566–9571.

11 X. Peng, F. Song, E. Lu, Y. Wang, W. Zhou, J. Fan and Y. Gao, *J. Am. Chem. Soc.*, 2005, **127**, 4170–4171.

12 W. Zhang, X. Zhao, W. Gu, T. Cheng, B. Wang, Y. Jiang and J. Shen, *New J. Chem.*, 2018, **42**, 18109–18116.

13 C. S. Abeywickrama and Y. Pang, *Tetrahedron Lett.*, 2016, **57**, 3518–3522.

14 V. S. Patil, V. S. Padalkar, K. R. Phatangare, V. D. Gupta, P. G. Umape and N. Sekar, *J. Phys. Chem. A*, 2011, **116**, 536–545.